

## Simulation of the Periodically Perturbed Separated and Reattaching Flow over a Backward-Facing Step

Z. Mehrez<sup>1</sup>, M. Bouterra<sup>1</sup>, A. El Cafsi<sup>1</sup>, A. Belghith<sup>1</sup> and P. Le Quéré<sup>2</sup>

<sup>1</sup> *Faculté des Sciences de Tunis-Campus Universitaire 1060 Tunis TUNISIE*

<sup>2</sup> *LIMSI-CNRS Bat. 508 - B.P. 133 - 91 403 Orsay Cedex FRANCE*

Email: [mehrez\\_zouhaier@yahoo.fr](mailto:mehrez_zouhaier@yahoo.fr)

(Received December 26, 2008; accepted June 15, 2009)

### ABSTRACT

In this work, the Large Eddy Simulation (LES) methodology is used to study the effects of a periodic perturbation introduced into a separated shear layer behind a backward-facing step. This study carried out by acting on the two parameters characteristics of the perturbation: frequency and amplitude. The obtained results reveal the existence of an optimum perturbation frequency value,  $St_p = 0.25$ , in terms of the reduced reattachment length. At this perturbation frequency value, we observed an increase in the vortical shedding frequency in the reattachment zone with a significant change of the structure of the flow. The value of the optimum frequency appears to be independent of the perturbation amplitude. At this frequency the maximum decrease of reattachment length is 50% and the maximum increase of vortical shedding frequency is 43 % compared to the unperturbed case.

**Keywords:** Large eddy simulation, backward-facing step, periodic perturbation, shedding frequency

### NOMENCLATURE

A	amplitude of perturbation	$u_i$	velocity vector
$f_p$	frequency of perturbation	u	longitudinal velocity
$f_s$	frequency of vortical shedding	$U_o$	maximum velocity in the inlet
H	computational domain width	v	transverse velocity
h	step height	t	time
Re	Reynolds nombre ( $U_o H / \nu$ )	x, y	Cartesian coordinates
P	pressure	$X_r$	reattachment length
$St_p$	Strouhal number of perturbation ( $f_p h / U_o$ )	$X_{r0}$	reattachment length for the non-perturbed flow
$St_s$	Strouhal number of vortical shedding ( $f_s h / U_o$ )		

### 1. INTRODUCTION

The flow separation and the subsequent reattachment caused by sudden expansion in flow geometry, such as a backward-facing step, occur in many engineering application. The performance of fluid machinery in industrial flows is greatly influenced by its presence. So, the control of flow separation is very interesting in the industrial field.

The problem of the flow over a backward-facing step continues to draw interest from CFD community because of its rich flow physics. As a result it has emerged as one of the benchmark problems. The backward-facing step flow has been extensively studied, but many aspects of the structure and the dynamics of this geometrically simple turbulent flow remain incompletely explained.

The suppression or desired control of separation phenomena has been addressed in the mechanics community for many decades. There has been much research interest on the periodically perturbed turbulent separated flow. Singurdson (1995), Chun and Sung (1996) are interested to the active control of the reattachment process, in which the enhancement of momentum transport across the separated shear layer plays a major role. Several authors are interested to the excitation of the instability and vortex formation inherent to the separated shear layer (Bhattacharjee *et al.*, 1986; Kiya *et al.*, 1997; Chun and Sung, 1998; Yoshioka *et al.*, 2001; Uruba *et al.*, 2007).

Among recent works, Hasegawa and kumagai (2008) developed a system of control using vortex generator jets with rectangular orifices for controlling the flow

separation of a two-dimensional diffuser. They confirmed that the proposed active separation control system could adaptively suppress flow separation for the flow fields caused by some changes in freestream velocity and the divergence angle of the diffuser.

The principal objective of this work is to modify the process of separation of the boundary layer and the phenomenon of shedding in order to control the separated and reattaching flow downstream of backward facing step, by using the Large Eddy Simulation methodology.

## 2. NUMERICAL SIMULATION

### 2.1 Basic Equations

The conservation equations describing the flow are the time-dependent, 2D Navier-Stokes equations and the conservation equation for a constant-property incompressible fluid.

The principle of LES is to explicitly simulate the large scales of a turbulent flow while parameterizing the small scales. Therefore, one begins by filtering the Navier-Stokes equations to obtain an equation for the large-scale motion. As usual, the non-linearity of the Navier-Stokes equations makes it impossible to obtain an exact closed equation for any filtered quantity, meaning that a term analogous to the Reynolds-Averaged Navier-Stokes (RANS) equations is produced and must be modeled.

For the flows considered here, the basic governing equations are written in dimensionless form as:

$$\frac{\partial \bar{u}_i}{\partial x_i} = 0$$

$$\frac{\partial \bar{u}_i}{\partial t} + \frac{\partial (\bar{u}_i \bar{u}_j)}{\partial x_j} = -\frac{\partial \pi}{\partial x_i} + \frac{\partial}{\partial x_j} \left( \frac{1}{\text{Re}} \frac{\partial \bar{u}_i}{\partial x_j} \right) - \frac{\partial (\tau_{ij})}{\partial x_j}$$

The bar in the LES equations denotes a filtered or large-scale flow quantity. The governing dimensionless parameter appearing in the above equations is the Reynolds number ( $\text{Re} = \frac{U_0 h}{\nu}$ ). When  $U_0$  denote the reference values of streamwise mean velocity and  $\nu$  is the kinematics viscosity. The modified pressure is given by:

$$\pi = \bar{p} + \frac{1}{3} \tau_{kk}$$

### 2.2. Subgrid Scale (SGS) Model

The Subgrid scale Reynolds stress is estimated by means of the eddy viscosity model:  $\tau_{ij} = 2\nu_t \bar{S}_{ij}$ , where

$$\bar{S}_{ij} = \frac{1}{2} \left( \frac{\partial \bar{u}_i}{\partial x_j} + \frac{\partial \bar{u}_j}{\partial x_i} \right)$$

is the strain rate tensor of the filtered flow field.  $\nu_t$  is the eddy viscosity.

Closure will be done when a model for the SGS is chosen. Throughout this paper, we have chosen a mixed subgrid-scale model, which is a part of one parameter ( $\alpha$ ) family of models proposed by [Ta Phuoc \(1994\)](#) and [Sagaut \(1998\)](#). These models take into account both the large and the small scales.

The turbulent eddy viscosity is given by a non linear combination of the second invariant of the shear stress tensor  $|\bar{S}|$ , the characteristic length scale  $\Delta$  and the kinetic energy  $q_c^2$  of the highest resolved frequencies:

$$\nu_t = c_m |\bar{S}|^\alpha (q_c^2)^{(1-\alpha)/2} \Delta^{(1+\alpha)}$$

This can be viewed as a non-linear combination of the Smagorinsky and the mixing-length model. For  $\alpha = 0$  and 1, the mixing length and the Smagorinsky models are retrieved, respectively.

When considering homogeneous isotropic turbulence and  $\alpha = 0.5$  (the value retained throughout this work), the theoretical value of the parameter  $c_m$  is found equal to 0.04 on the basis of an equilibrium assumption between the dissipation and energy-transfer rates. The characteristic length scale is usually chosen to be  $\Delta = \sqrt{\Delta x \Delta y}$ , where  $\Delta x$  and  $\Delta y$  are mesh sizes in the  $x$ - and  $y$ -directions respectively. The sec invariant of the shear stress tensor is given by:

$$|\bar{S}| = \sqrt{S_{ij} S_{ij} / 2}$$

and the kinetic energy  $q_c^2$  is obtained by the scale similarity assumption and by means of a double-filtering technique:  $q_c^2 = \frac{1}{2} (\bar{u}_i - \hat{u}_i)^2$ , where  $(\hat{\cdot})$  represents a filter with a cut-off length of  $2\Delta$ . The explicit filter used here is a local weighted-average

$$\hat{u}_i = \frac{1}{4} \bar{u}_{i-1} + \frac{1}{2} \bar{u}_i + \frac{1}{4} \bar{u}_{i+1}.$$

The mixed Subgrid scale model is a self-adapted model because the eddy viscosity vanishes automatically at the wall and in the regions of the flow where all the structures are well resolved.

### 2.3 Numerical Resolution

The calculations have been performed using a Navier-Stokes equations solver, which was developed at LIMSI (Laboratoire d'Informatique pour la Mécanique et les Sciences de l'Ingénieur-Orsay Paris) for the simulation of complex turbulent flows.

The time integration is performed using a time-splitting algorithm, also known as a prediction-projection algorithm, which allows one to decouple pressure from velocity. Assuming all quantities known at time  $n\Delta t$ , the solution at time  $(n+1)\Delta t$  is obtained as follows:

An intermediate velocity field  $U^*$  is first computed using a second-order time scheme. This time stepping combines a second order backward Euler scheme for

the diffusion terms, with an explicit second-order Adams-Bashforth extrapolation for the non-linear terms, taking into account known pressure field. This step reads:

$$\frac{3U^* - 4U^n + U^{n-1}}{2\Delta t} + 2(U\Delta U)^n - (U\Delta U)^{n-1} = -\Delta p^n + \frac{1}{Re}\nabla^2 U^*$$

- In the second step, this intermediate velocity field is projected on to the subspace of divergence free vector field using the Helmholtz decomposition theorem. This step reads:

$$\frac{3(U^{n+1} - U^*)}{2\Delta t} = -\nabla(\underbrace{p^{n+1} - p^n}_{\phi})$$

- It is accomplished by taking the divergence of equation giving rise to a Poisson's type equation for the incremental pressure:  $\Delta\phi = \frac{3}{2\Delta t}\nabla U^*$
- This equation is solved with a multigrid algorithm, in which the presence of internal blockings is automatically taken into account
- Once the pressure field is obtained, the new quantities at  $n+1$  are given by:

$$\begin{cases} p^{n+1} = \phi + p^n \\ U^{n+1} = U^* - \frac{2}{3}\Delta t\nabla\phi \end{cases}$$

The space discretization uses a centred scheme for the diffusive fluxes and a second order upwind finite difference method by means of a Quadratic Upstream Interpolation Convective Kinematics (QUICK) scheme for the convective terms, as proposed by Leonard (1988).

### 3. FLOW GEOMETRY AND BOUNDARY CONDITIONS

The computations were performed on a 2D computational domain (represented in the Fig. 1) whose streamwise length, behind the step was set equal to  $X_m = 14h$ .

At the inlet, a boundary layer velocity profile is considered:

$$\begin{aligned} u(y) &= 1.92(y/10)^{0.25} & \text{for } 0.33 \leq y/H \leq 0.75 \\ u(y) &= 1 & \text{for } 0.75 \leq y/H \leq 1 \end{aligned}$$

At the outlet, the  $u$ -velocity is calculated from global continuity together with a zero gradient boundary condition for both  $u$  and  $v$ . No-slip conditions are prescribed at the body surfaces ( $u=v=0$ ). At the upper boundaries, symmetry conditions simulating a frictionless wall are used ( $v = \frac{\partial u}{\partial y} = 0$ ).

Chun and Sung (1998), Yoshioka *et al.* (2001) experimentally introduced a periodic perturbation by pulsating jet (blowing and suction of the fluid) at the edge of the step. In this study, we have simulated such a perturbation by introducing a local velocity  $u = A \sin 2\pi f_p t$  (Fig. 1).

## 4. RESULTS AND DISCUSSION

### 4.1 Grid and Time Step Refinement

In this work, all refinement tests are undertaken on non-perturbed flow. The grid refinement tests have been performed using three uniform fine grids:  $66 \times 33$ ,  $104 \times 66$  and  $130 \times 75$  for  $Re=33000$ . Results showed that when we pass from the first grid to the second, the reattachment length  $X_r/h$  undergoes an increase of 7.1%. When we pass from the second grid to the third, the reattachment length undergoes an increase of only 1.12%. We conclude that the grid of  $104 \times 66$  gives a good compromise between precision and calculation time and is sufficient to carry out a numerical study of this flow.

The time-step  $\Delta t$  is conditioned by the Courant-Friedrich-Lewy (CFL) criterion. The adjustment of its value is undergone using the optimal  $104 \times 66$  grid. Some preliminary runs showed that the dimensionless time interval  $tU_o/H = 400$  is large enough to reach the asymptotic regime considered in the current study. Accordingly, we have done three simulations with  $\Delta t$  equal to  $8 \cdot 10^{-3}$ ,  $4 \cdot 10^{-3}$ , and  $10^{-3}$ . Obtained reattachment length values are respectively;  $X_r/h = 6.7, 7.2$  (i.e an increase of 6.94% with respect to the previous value) and 7.28 (i.e an increase of only 1.1%). Basing on these data, and calculation-time consuming considerations, the time-step value is finally set to  $4 \cdot 10^{-3}$ . It's worth to remind here, that for  $\Delta t = 10^{-3}$ , 400000 time steps are necessary to reach the asymptotic regime. This number falls down to 100000 for  $\Delta t = 4 \cdot 10^{-3}$ .

### 4.2 Simulation of the Flow without Perturbation

In this section the Reynolds number is fixed at  $Re=33000$ . Figure 2a shows the iso-vorticity lines. In the wake four different zones exist: The recirculation zone, the shear layer above the recirculation, the reattachment region and the redevelopment zone, when a new boundary layer develops. It is generally known that the fluid detaches in the step edge forming the shear layer governed by the instability. Perturbations are amplified and lead up to shear layer roll-up into spanwise coherent vortical structures. These vortices detach and convect downstream. In the reattachment zone the grown vortices are affected by the lower wall and decay in the restructuring flow. In this study we will refer to the frequency of detachment of these vortices as shedding frequency.

The Fig. 2b represents the iso-stream function lines. We can note the existence of recirculation zone formed by two contra-rotating vortexes. The value of the time-mean reattachment length (mentioned in Fig. 2b by a triangle) in the experiment of Sung and Chun (1998) is  $X_r = 7.4h$ , our simulations give a value of  $X_r = 7.2h$ . The agreement between the computation and the experiment is rather good.

Figure 3 shows the temporal evolution of the longitudinal component of the velocity in the reattachment zone (Fig. 3a) and its spectrum (Fig. 3b).

As can be seen, the velocity clearly oscillates about average value during the whole time interval, indicating that this zone is the seat of vortical motion. This motion is responsible for vortical shedding phenomenon. The spectrum of the longitudinal velocity shows predominant frequency that defines the shedding frequency  $f_s$ . In this case of non-perturbed flow the value of the dimensionless frequency, presented by a Strouhal number of shedding is  $St_s = 0.14$ .

### 4.3 Simulation of Perturbed Flow

#### 4.3.1 Effects of Perturbation Frequency

This study carried out by fixing the perturbation amplitude at  $A = 0.3U_0$ .

##### Reattachment Length

The normalized reattachment length,  $X_r/X_{r0}$  is plotted in Fig. 4 as a function of the Strouhal number of perturbation  $St_p$  for Reynolds number  $Re = 33000$ . The experimental data of Chun and Sung (1998) and the numerical works using the  $k-\epsilon-f_\mu$  model (Rhee *et al.* 2000) are also included for comparison.  $X_r$  varies by variation of the perturbation frequency. The minimum observed at the optimum frequency,  $St_p = 0.25$ , in terms of the reduced reattachment length. The agreement between the computation and the experiment is satisfactory, in particular, the optimum frequency ( $St_p = 0.25$ ) in the experiment is clearly reproduced by the present model. It is known that the shear layer above the recirculation zone is the seat of formation of coherent vortical structures. These vortices that are convecting downstream are responsible for the entrainment out of the recirculation zone. By stimulating their growth through applying a perturbation, the increased shear layer growth rate leads to a significant reduction of the recirculation zone size. The maximum reduction is obtained at the optimum frequency of perturbation  $St_p=0.25$ .

Figure 5 shows the variation of normalized reattachment length,  $X_r/X_{r0}$  against  $St_p$  for different Reynolds numbers. In all  $Re$  cases, the reattachment length decreases with increasing  $St_p$  before it reaches a minimum at  $St_p = 0.25$ , and then increase again. The optimal value of the perturbation frequency is independent of the Reynolds number. We can note also that, for different  $St_p$  values, the effect of perturbation on the reattachment length weakens by increasing  $Re$ . So, the control of the flow becomes more difficult by increasing  $Re$ .

##### Vortical Shedding Frequency

Figure 6 shows the Strouhal number of shedding  $St_s$  against  $St_p$ . The shedding frequency varies by variation of perturbation frequency. The pronounced peak is observed at the optimum frequency ( $St_p=0.25$ ). This result shows that the shedding phenomenon is modified following the modifications of the separation of the fluid by perturbation.

Physically, there is a relation between the enhancement of shedding frequency and the reduction of the reattachment length. Indeed, following the enhancement

of the turbulent intensity level, in the separation, by application of perturbation, the shear layer growth rate enhances, this decreases the reattachment length, reduces the residence time and increases the shedding frequency.

##### Mean Flow Field

Figure 7a shows the iso-vorticity lines. We can note that the curvature to the bottom of the field lines is more interesting by perturbation; this reduces the size of the recirculation zone. This result is explained by an increase in the shear layer growth rate. At the optimum perturbation frequency the effect becomes more significant. The same result is also confirmed by the streamlines (Fig. 7b). The weak effect of perturbation in the others cases  $St_p = 0.05$  and  $St_p = 1$ , particularly in the reattachment reduction, explained in the low-frequency perturbation by the effect of large scale vortex motion appears after the flow reattaches, which inhibits the promotion of reattachment length. In the higher perturbation frequency, the vortices generated by perturbation decay fast without affecting the shear layer. Obi *et al.* (1997) considered the perturbation with too high frequency decay too fast, that with too low frequency provides only weak effect before the flow reattachment. The existence of the optimum frequency range as a consequence of these two different reasons.

#### 4.3.2 Effects of Perturbation Amplitude

In this section the Reynolds number value is fixed at  $Re = 33000$ .

##### Reattachment Length and Vortical Shedding Frequency

The normalized reattachment length  $X_r/X_{r0}$  as a function of Strouhal number of perturbation  $St_p$ , for various normalized amplitude perturbation  $A/U_0$ , is plotted in the Fig. 8. All the curves show the same general features. The reattachment length, for all cases, reaches a minimum value at the  $St_p=0.25$ . The optimum value of perturbation frequency is independent of the amplitude perturbation.

The reattachment length decreases with increasing the perturbation amplitude at the optimum frequency (see Fig. 9a) until  $A = 1.55U_0$ . Starting from this point, no significant effects of the variation of amplitude are observed. The maximum reduction of  $X_r$ , compared to non-perturbed case, is 50 %. This is accompanied by the increase of the vortical shedding frequency  $St_s$  (see Fig. 9b). The shedding frequency augments by increasing the perturbation amplitude until reaching a constant value from the amplitude  $A = 0.4U_0$ . The maximum enhancement of the shedding frequency, compared to non-perturbed case, is 43 %. These results can be explained by enhancement of turbulence level in the separation with augmentation of perturbation amplitude at the optimum frequency.

##### Mean Flow Field

To see the effect of the amplitude on the mean flow, the iso-stream lines and the iso-vorticity lines are displayed at the optimum perturbation frequency for four values of amplitude:  $A = 0$ ,  $A = 0.3U_0$ ,  $A=0.6U_0$ ,

and  $A = 1.2U_0$  (Fig. 10). The iso-vorticity lines show that the structure of vortex in the shear layer becomes more intense and the curvature of the shear layer towards the bottom wall is more significant by increasing the perturbation amplitude (Fig. 10a). Consequently, the size of the recirculation zone and the reattachment length decrease (Fig. 10b). We can note also the intensification of large scale vortex and the weakening of the small structure in the recirculation zone by augmentation of the perturbation amplitude. The dashed line in Fig. 10b shows the reduction of the size of the recirculation zone, and the triangles indicate the reattachment length.

## 5. CONCLUSION

The influence of a periodic perturbation on the flow over a backward facing step is investigated by the LES methodology. The results which we obtained show the presence of an optimum perturbation frequency value,  $St_p = 0.25$ , in terms of the reduction of the time-mean reattachment length. Our calculations are in good agreement with some experimental results. At the optimum frequency, we note a significant increase of the shedding frequency in the reattachment zone. The augmentation of the perturbation amplitude at the optimum frequency: i) increases the vortical intensity in the shear layer, ii) decreases the time mean reattachment length and iii) increases the shedding frequency. The maximum reduction of the reattachment length is 50 % and the maximum rise of the shedding vortical frequency is 43% compared to unperturbed case. These results show the effectiveness of periodic perturbation for the control of separated and reattaching flow.

## REFERENCES

- Battacharjee, S., B. Scheelke and T.R. Troutt (1986). Modification of vortex interaction in a reattaching separated flow. *AIAA* 24, 623-629.
- Chun, K.B. and H.J. Sung (1998). Visualization of a locally- forced separated flow over a backward-facing Step. *Exp. Fluids* 25, 417-426.
- Chun, K.B. and H.J. Sung (1996). Control of turbulent separated flow over a backward-facing Step by local forcing. *Exp. Fluids* 21, 133-142.
- Hasegawa, H and S. kumagai (2008). Adaptive Separation Control System Using Vortex Generator Jets for Time-Varying Flow. *Journal of Applied Fluid Mechanics* 2, 9-16.
- Kiya, M., M. Shimizu and O. Mochizuki (1997). Sinusoidal forcing of a turbulent separation bubble. *J. of Fluid Mechanics* 330, 349-374.
- Leonard, B.P. (1988). Simple high accuracy resolution program for convection modelling of discontinuities, *Int. J. for Num. Methods in fluids* 8, 1291-1318.
- Obi, S., N. Ishibashi and S. Masuda (1997). *The Mechanism of Momentum Transfer Enhancement in the Periodically Perturbed Turbulent Separated Flow. In: Turbulence, Heat and mass Transfer 2*, Hanjalic, K. and T.W.J. Peeters (Eds.). Delft University Press, Delft, 835-844.
- Rhee, G.H. and H.J. Sung (2000). Turbulent Numerical prediction of locally forced separated and reattaching flow, *Fluid Dynamics Research* 26, 421-436.
- Sagaut, P.(1998). Introduction à la simulation des grandes échelles pour les écoulements de fluide incompressible. Book. Math. Springer-Verlag, Collection Mathématiques et applications 30, 282 pages.
- Sigurdson, L.W. (1995). The structure and control of a turbulent reattaching flow. *J. of Fluid Mechanics* 298, 139-165.
- Ta Phuoc, L. (1994). Modèles de sous maille appliqués aux écoulements instationnaires décolles, DGA/DRET, *Journée thématique DRET: Aérodynamique instationnaire turbulente, aspects numériques et expérimentaux*, France.
- Uruba, V., P. Jonas and O. Mazur (2007). Control of a channel-flow behind a backward-facing step by suction/blowing. *Int. J. of Heat and Fluid Flow* 28, 665-672.
- Yoshioka, S., S. Obi and S. Masuda (2001). Organized vortex motion in periodically perturbed turbulent flow over a backward-facing step. *Int. J. Heat Fluid Flow* 22, 301-307.

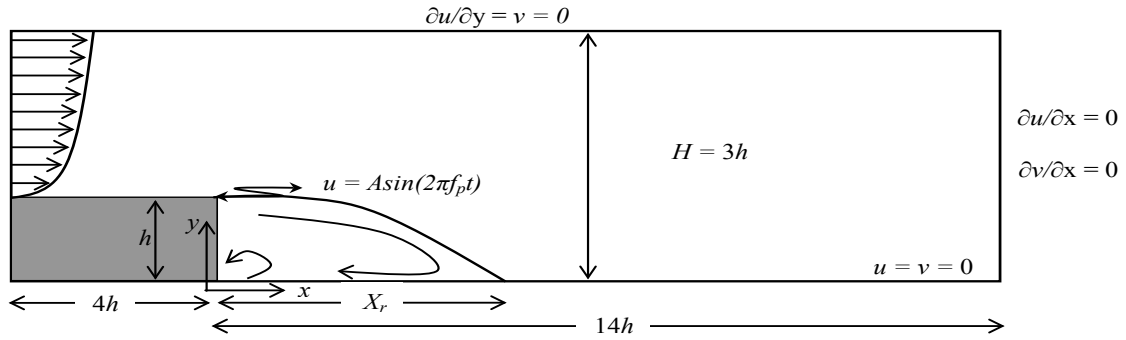


**Fig. 1.** Geometric configuration of computational domain.

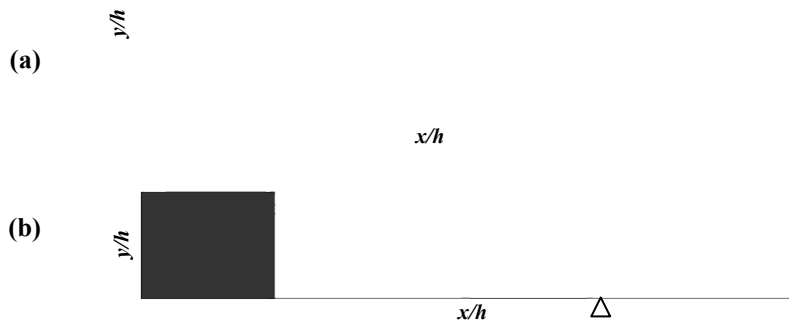


**Fig. 2.** Distributions of: (a) Iso-vorticity lines, (b) Iso-stream function lines.  $Re=33000$ , without perturbation.

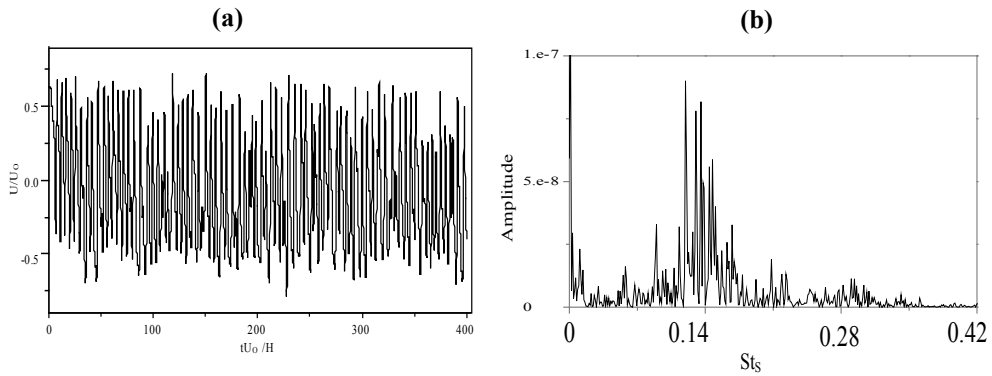


**Fig. 3.** (a) Temporal evolution of longitudinal velocity, (b) Spectrum of longitudinal velocity. In the reattachment zone,  $Re = 33000$ , without perturbation.

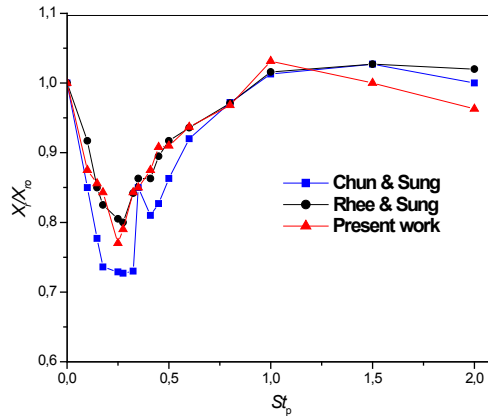


**Fig. 4.** Normalized reattachment length  $X_r/X_{r0}$  against  $St_p$ ,  $Re = 33000$ ,  $A = 0.3U_0$ .

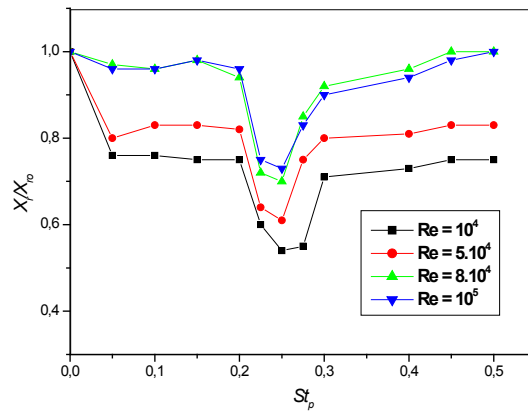


**Fig. 5.** Normalized reattachment length  $X_r/X_{r0}$  against  $St_p$  for different Reynolds numbers.

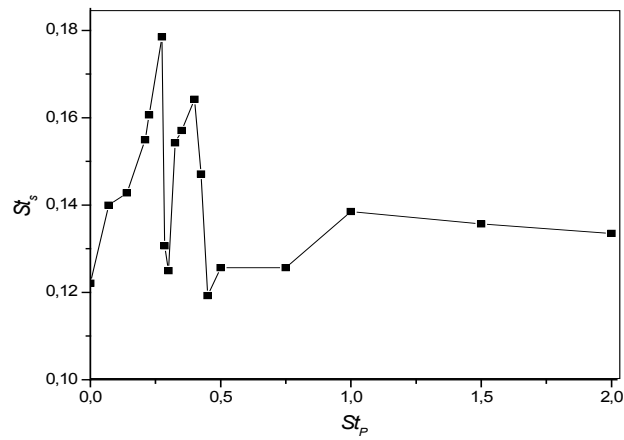


**Fig. 6.** Shedding frequency  $St_s$  against perturbation frequency  $St_p$ ,  $Re = 33000$  and  $A = 0.3U_0$ .

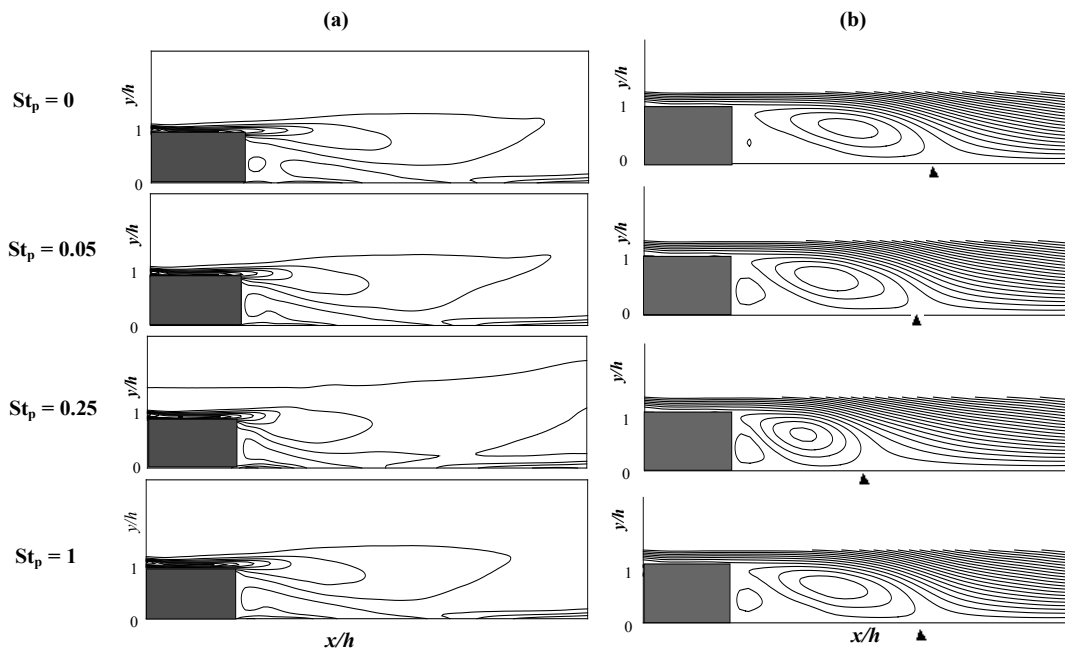


**Fig. 7.** Distributions of: (a) Iso-vorticity lines (b) Iso-stream function lines for different perturbation frequency,  $Re = 33000$ .

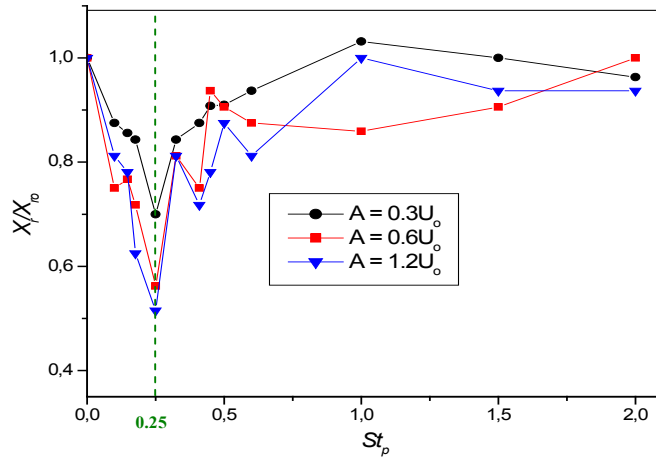


**Fig. 8.** Normalized reattachment length  $X_r/X_{r0}$  against  $St_p$  for different perturbation amplitudes,  $Re = 33000$ .

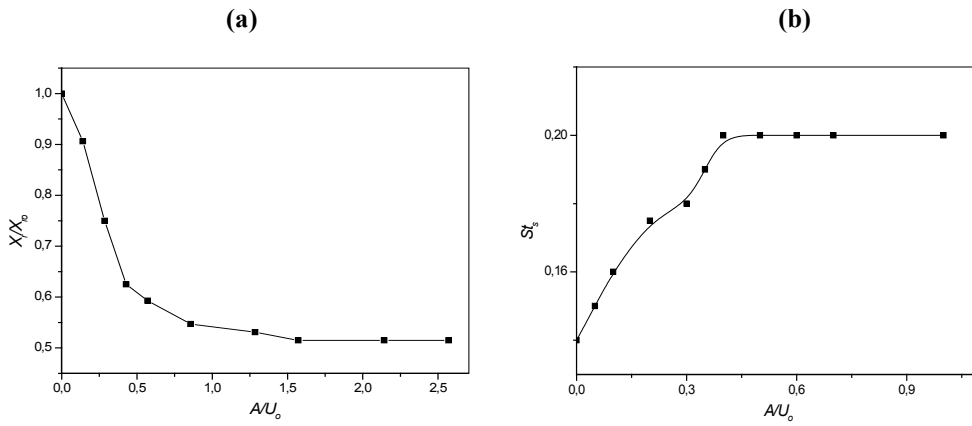


**Fig. 9.** (a)  $X_r/X_{r0}$  against  $A/U_0$ , (b)  $St_s$  against  $A/U_0$ ,  $Re = 33000$  and  $St_p = 0.25$ .

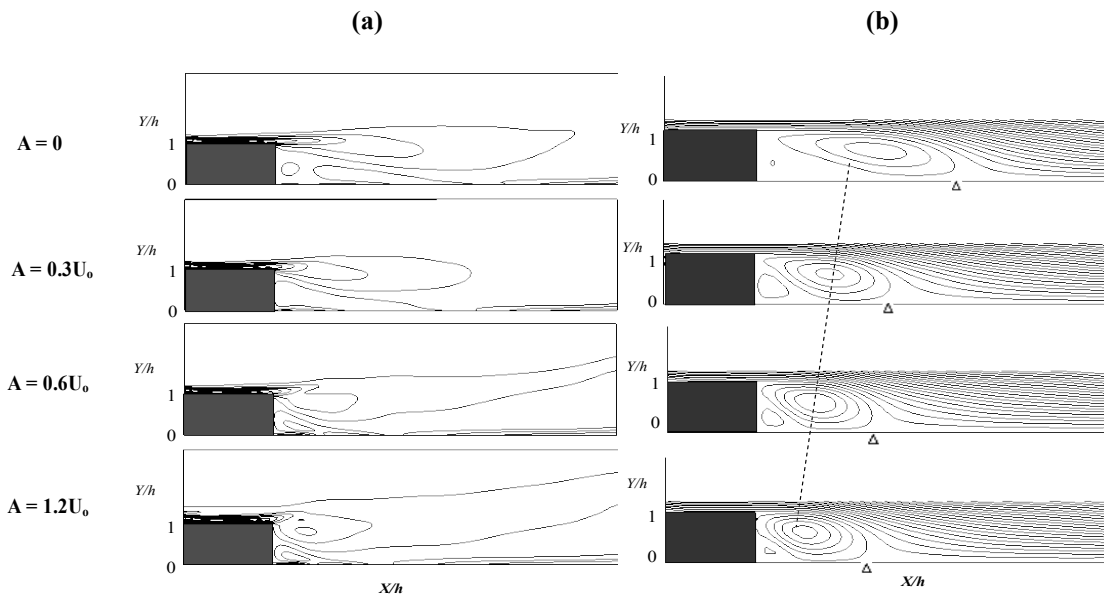


**Fig. 10.** Distributions of: (a) Iso-vorticity lines (b) Iso-stream function lines for different perturbation amplitudes,  $Re = 33000$  and  $St_p = 0.25$ .